CSIAM Trans. Appl. Math.
doi: 10.4208/csiam-am.SO-2024-0044

Vol. **x**, No. x, pp. 1-23
xx 2025

An Efficient Iterative Convolution-Thresholding Method for Image Inpainting

Caixia Nan[1], Zhonghua Qiao[2] and Dong Wang[3,4,*]

[1] *School of Mathematical Sciences, Ministry of Education Key Laboratory of NSLSCS, Nanjing Normal University, Nanjing 210023, P.R. China.*
[2] *Department of Applied Mathematics, The Hong Kong Polytechnic University, Hung Hom, Kowloon, Hong Kong SAR, P.R. China.*
[3] *School of Science and Engineering, The Chinese University of Hong Kong (Shenzhen), Shenzhen 518172, P.R. China.*
[4] *Shenzhen International Center for Industrial and Applied Mathematics, Shenzhen Research Institute of Big Data, Shenzhen 518172, P.R. China.*

Received 11 September 2024; Accepted 16 June 2025

Abstract. Variational methods have been developed for image inpainting, which involve minimizing an objective functional consisting of the regularization term and the fidelity term. The fidelity term controls the consistency of the restored region with the original image, while the regularization term smooths the boundary of the region. In this paper, we develop an efficient iterative convolution-thresholding method to solve variational approach-based image inpainting problems. In the proposed method, the region is represented by its indicator function, and the regularization term is approximated by the heat kernel convolution with the indicator function. Based on this approximation, we derive an efficient iterative method to update the indicator function only within the damaged region by alternating the convolution and thresholding steps, relying on a relaxation and linearization procedure. Extensive numerical experiments demonstrate the simplicity and efficiency of the proposed method.

AMS subject classifications: 68U10, 68T10, 62P10, 62H35

Key words: Iterative convolution-thresholding method, heat kernel, image inpainting.

1 Introduction

Image inpainting plays a crucial role in the field of image processing, encompassing the restoration of missing or damaged areas within images by leveraging information from surrounding areas. This technique finds wide-ranging practical applications, such as the

*Corresponding author. *Email addresses:* nancaixia@njnu.edu.cn (C. Nan), zhonghua.qiao@polyu.edu.hk (Z. Qiao), wangdong@cuhk.edu.cn (D. Wang)

revitalization of weathered artworks by museum artists [19], the elimination of scratches from old photographs [6], the manipulation of scenes in photographs [16], the restoration of motion pictures [26], and numerous others. The diverse applications of image inpainting underscore its indispensability as a tool for visual restoration and enhancement, showcasing its versatility and profound utility in image processing.

The primary challenge in image inpainting lies in generating images that exhibit sharp edges, intricate texture patterns, or clear structures from the available data [7]. Various useful methods for image inpainting have been developed, such as the exemplar-based methods [8], texture synthesis methods [22], deep neural networks methods [28], and variation-based methods [11]. Variation-based methods usually consider proper representations of the interfaces between domains with binary intensities, the approximate of an objective functional, and efficient methods to optimize the approximate objective functional. In this paper, we focus on developing an effective approximation and efficient algorithm for the variation-based approaches.

As for variation or partial differential equations based approaches, Bertalmio *et al.* [4] leveraged the Navier-Stokes equation, typically employed in fluid dynamics, to reconstruct missing image regions. This approach, rooted in nonlinear PDEs, incorporates a fidelity term to ensure fidelity to the original image. Further studies have validated the mathematical underpinnings of these fluid dynamic models [18] and their efficacy in preserving image structures [3].

Subsequently, Chan and Shen [11] introduced the total variation (TV) for image inpainting, which extends the classical TV denoising model [39]. However, the TV model encountered challenges in maintaining connectivity within images. This limitation spurred the emergence of enhanced TV models, including total generalized variation [45], Shannon TV model [1], and Condat's model [14], which exhibit superior edge and structure preservation compared to the traditional TV model. These models are usually solved by optimization approaches, such as the alternating direction method (ADM) [10], operator splitting method [36], iterative Lagrange multiplier method [52] and dual formulation [14, 45]. But they typically contain many parameters in their numerical schemes, leading to a complicated parameter tuning process.

Addressing the connectivity issue, the integration of Euler's elastica curvature model proved effective in reestablishing damaged image contours. Esedoglu and Shen extended the application of the Mumford-Shah (MS) model from image segmentation and denoising [35] to greyscale image inpainting [21]. While the MS model often resulted in overly smooth image restorations, the introduction of the Mumford-Shah-Euler (MSE) model, which incorporates Euler's elastica curvature term, overcame this limitation and demonstrated enhanced performance in digital inpainting tasks [24]. These models essentially are based on the level set representation of interface and solved by the gradient flow system, which can effectively handle complex geometries and topological changes naturally due to its implicit representation of curvature or boundaries. The augmented Lagrangian method (ALM) [43], Lagrange multiplier approach [23] and operator splitting algorithms [15] are used for the Euler's elastica model. However, it is usually computa-

tionally expensive, sensitive to the selection of parameters, and requires reinitialization techniques.

Recent advancements have seen the integration of phase field models in image inpainting, such as the modified Cahn-Hilliard (MCH) model, known for its efficacy in reconstructing large damaged areas through a fourth-order PDE approach [5]. Wang *et al.* [51] proposed a novel method employing the Allen-Cahn equation with a phase-dependent fidelity term, showcasing efficient local image inpainting. Additionally, Bai *et al.* [2] introduced the Ginzburg-Landau model combined with the H^{-1}-fidelity term, demonstrating effectiveness in intricate image regions. These models can generally be effectively solved by structure-preserving stable methods, such as the convex splitting-based method [37], the exponential time integration method [30], and the scalar auxiliary variable-based methods [2, 41, 42].

The challenge of inpainting images naturally aligns with interface problems, allowing segmentation methods to be extended to address inpainting tasks. Notably, the level-set method [27, 29], initially devised for image segmentation purposes, has found successful applications in image inpainting [17, 21]. In this paper, we focus on the recently developed iterative convolution-thresholding method (ICTM) [32, 48, 49]. The inspiration for this method comes from a threshold dynamics method developed in [20, 33], which simulates the motion by mean curvature for an interface. The basic procedure involves representing the interface using an indicator function, approximating the objective functional in a concave way, and alternating a convolution and a thresholding step to update the interface. Liu *et al.* [31] further developed a minimization algorithm by combining the ICTM with the local variance force term (ICTM-LVF), and the numerical experiments illustrated its effectiveness for image segmentation with noise. The ICTM has the property on the monotonic decay of the objective functional which implies the stability of the iteration. In addition, one can observe that the results are achieved using ICTM with much fewer iterations and shorter time compared to other methods from [31, 48, 49], and the convergence is verified in [50]. The idea has also been extended to target-valued image denoising [38], and topology optimization [9, 12, 13, 25].

In this paper, we develop an efficient ICTM to restore the damaged binary, greyscale, and color images. We first approximate the regularization term using heat kernel convolution in a concave way and then reformulate the fidelity term in a linear form. Next, the relaxation and linearization approaches introduced in [20] are applied to the approximate optimization problem to derive the ICTM. Furthermore, the stability property based on ICTM is theoretically proved. To highlight the efficiency of ICTM for image inpainting, we consider several well-known approaches for comparison, such as the convex splitting method for the MCH model, the ALM, and the operator splitting method for Euler's elastica model. Numerical results between different methods demonstrate that the ICTM achieves high efficiency.

The organization of this paper is as follows. In Section 2, we present the approximate model. In Section 3, we derive the ICTM for inpainting problems and theoretically prove the stability. In Section 4, we present several numerical examples to illustrate the effi-

ciency and accuracy of the ICTM in image inpainting. We then draw some conclusions in Section 5.

2 The approximate model

Variational approaches for binary image inpainting can be treated as the reconstruction of the interface inside the damaged region such that the intensity inside the damaged domain is consistent with that in the outside of the damaged region. One usually considers minimizing an objective functional consists of the regularization term and the fidelity term. Considering the binary image with two constant intensities defined in two regions Ω_1 and Ω_2, the specific expression is given as

$$E=\mu|\Omega_1\cap\Omega_2|+\lambda\int_{\Omega\setminus D}(u-f)^2dx, \tag{2.1}$$

where $|\Omega_1\cap\Omega_2|$ is the length of the interface between two regions with different intensity, μ and λ are positive constants, f represents the given damaged image, and D denotes the damaged domain. The MCH equation proposed in [5] can be treated as a modified gradient flow where one considers the H^{-1} gradient flow of the regularization term and a L^2 gradient flow of the fidelity term, based on a phase field representation of the interface and an approximation to the interface length with a small parameter ϵ.

Essentially, the principle of the binary inpainting problem is to reconstruct the interface between two regions in the damaged region and keep the intensity outside of the damaged region unchanged. Motivated by the ICTM for image segmentation [48,49], we use indicator functions of the domains to implicitly represent the interface. Denote u as the characteristic function of Ω_1,

$$u(x):=\begin{cases}1, & \text{if} \quad x\in\Omega_1,\\ 0, & \text{otherwise},\end{cases} \tag{2.2}$$

and $1-u$ as the characteristic function of Ω_2.

As illustrated in [20,34], when $\tau\ll 1$, the measure of $\Omega_1\cap\Omega_2$ in (2.1) can be approximated by

$$|\Omega_1\cap\Omega_2|\approx\sqrt{\frac{\pi}{\tau}}\int_\Omega uG_\tau*(1-u)\,dx, \tag{2.3}$$

where $*$ denotes the convolution and G_τ is the heat kernel in 2-dimensional space

$$G_\tau(x)=\frac{1}{4\pi\tau}\exp\left(-\frac{|x|^2}{4\tau}\right). \tag{2.4}$$

The original objective functional (2.1) is then approximated by

$$E^\tau(u)=\mu\sqrt{\frac{\pi}{\tau}}\int_\Omega uG_\tau*(1-u)dx+\lambda\int_{\Omega\setminus D}(u-f)^2dx. \tag{2.5}$$

Denote the admission set B as

$$B := \{u \in BV(\Omega,R) \,|\, u(x) \in \{0,1\}, \forall x \in \Omega\},$$

where $BV(\Omega,R)$ denotes the bounded-variation functional space. We consider the approximate inpainting problem by solving

$$u^{\tau,*} = \arg\min_{u\in B} E^{\tau}(u). \tag{2.6}$$

3 Derivation of the method

In this section, we derive an unconditional stable efficient ICTM for problem (2.6). Note that the second term in $E^{\tau}(u)$ is strictly convex in u, one can not directly use the linearization and relaxation way to derive a method to unconditionally decay the objective function. Using the fact that $(u(x))^2 = u(x), \forall u \in B$, we consider the following equivalent problem:

$$u^{\tau,*} = \arg\min_{u\in B} \tilde{E}^{\tau}(u), \tag{3.1}$$

where

$$\tilde{E}^{\tau}(u) = \mu\sqrt{\frac{\pi}{\tau}}\int_{\Omega} uG_{\tau} * (1-u)dx + \lambda\int_{\Omega}(1-\chi_D)\left(u(1-2f)+f^2\right)dx, \tag{3.2}$$

and χ_D is the indicator function of the damaged domain D, i.e. $\chi_D(x)=1$ when $x\in D$ and $\chi_D(x)=0$ when $x\in\Omega\setminus D$.

Denote the convex hull of B as $\mathcal{K}$, where

$$\mathcal{K} := \{u(x) \in BV(\Omega,R) \,|\, u(x) \in [0,1], \forall x \in \Omega\}.$$

We first summarize some properties of $\tilde{E}^{\tau}(u)$ and the admissible set in the following lemma, which can also be referred to similar results in [20, 49].

Lemma 3.1. *Assume $\tau > 0$, then the following properties hold for the functional $\tilde{E}^{\tau}(u)$ defined and the admissible set:*

(i) $\tilde{E}^{\tau}(u)$ is concave with respect to u on $\mathcal{K}$.

(ii) The Fréchet derivative of $\tilde{E}^{\tau}(u)$ with respect to $u\in\mathcal{K}$ is

$$\frac{\delta\tilde{E}^{\tau}(u)}{\delta u} = \mu\sqrt{\frac{\pi}{\tau}}G_{\tau} * (1-2u) + \lambda(1-\chi_D)(1-2f).$$

(iii) B is the boundary of $\mathcal{K}$.

Proof. (i) Using the semi-group property of heat kernel [46], one can conclude that

$$\begin{aligned}\tilde{E}^\tau(u) &= \mu\sqrt{\frac{\pi}{\tau}}\int_\Omega uG_\tau*(1-u)dx+\lambda\int_\Omega(1-\chi_D)\big(u(1-2f)+f^2\big)dx\\ &= \mu\sqrt{\frac{\pi}{\tau}}\int_\Omega(G_{\tau/2}*u)(1-G_{\tau/2}*u)dx+\lambda\int_\Omega(1-\chi_D)\big(u(1-2f)+f^2\big)dx.\end{aligned}$$

It is then easy to see that the first term is concave and the second term is linear in u.

(ii) The variation can be computed as follows:

$$\begin{aligned}\left\langle\frac{\delta\tilde{E}^\tau(u)}{\delta u},v\right\rangle &= \lim_{\epsilon\to0}\frac{\tilde{E}^\tau(u+\epsilon v)-\tilde{E}^\tau(u)}{\epsilon}\\ &= \mu\sqrt{\frac{\pi}{\tau}}\int_\Omega vG_\tau*(1-2u)dx+\lambda\int_\Omega(1-\chi_D)(1-2f)vdx,\end{aligned}$$

where $\langle f,g\rangle$ denotes $\int_\Omega fg\,dx$ and we use the fact that

$$\int_\Omega vG_\tau*(-u)dx=\int_\Omega uG_\tau*(-v)dx.$$

(iii) This can be proved by a direct computation. □

Because the fact that the minimizer of a concave functional on a convex set can always be attained at the boundary, from above properties, one can consider the following equivalent problem to (3.1):

$$u^{\tau,*}=\arg\min_{u\in\mathcal{K}}\tilde{E}^\tau(u). \tag{3.3}$$

To solve (3.3), given an initial guess u^0, we use the property of the concavity of $E^\tau(u)$ to generate an iterative sequence

$$u^1,u^2,\cdots,u^k,\cdots$$

such that

$$u^{k+1}=\arg\min_{u\in\mathcal{K}}L^\tau(u,u^k), \tag{3.4}$$

where

$$L^\tau(u,u^k)=\tilde{E}^\tau(u^k)+\left\langle u-u^k,\mu\sqrt{\frac{\pi}{\tau}}G_\tau*(1-2u^k)+\lambda(1-\chi_D)(1-2f)\right\rangle$$

is the linearization of $\tilde{E}^\tau(u)$ at $u=u^k$. Then (3.4) is equivalent to solve

$$u^{k+1}=\arg\min_{u\in\mathcal{K}}\int_\Omega u\phi^k\,dx,$$

where

$$\phi^k = \mu\sqrt{\frac{\pi}{\tau}}G_\tau * (1-2u^k) + \lambda(1-\chi_D)(1-2f).$$

The linear optimization problem (3.4) can then be solved pointwisely by a simple thresholding step as follows to generate u^{k+1}:

$$u^{k+1}(x) = \begin{cases} 1, & \text{if } \phi^k(x) < 0, \\ 0, & \text{otherwise.} \end{cases} \tag{3.5}$$

Note that

$$\phi^k(x) = \mu\sqrt{\frac{\pi}{\tau}}\big(G_\tau * (1-2u^k)\big)(x), \quad \forall x \in D,$$

the thresholding step for $x \in D$ can be further simplified by

$$u^{k+1}(x) = \begin{cases} 1, & \text{if} \quad \big(G_\tau * (1-2u^k)\big)(x) < 0, \\ 0, & \text{otherwise,} \end{cases} \quad \forall x \in D. \tag{3.6}$$

Considering λ to be sufficiently large to guarantee the image outside the damaged domain is consistent with the original image, the thresholding for $x \in \Omega \setminus D$ is then dominated by the values of f. When we consider binary inpainting with $f(x) \in \{0,1\}$, one can directly have that the thresholding step for $x \in \Omega \setminus D$ is equivalent to setting $u(x) = f(x)$ for any $x \in \Omega \setminus D$.

The algorithm is summarized into Algorithm 1.

Algorithm 1: The ICTM for Approximating Minimizers of (3.3).

Input: u^0: Initial guess, $\tau > 0, tol > 0$, a given image f with damaged region D.

Output: $u^* \in \mathcal{B}$.

while $\|u^{k+1} - u^k\|_2 > tol$ **do**

1. Compute $G_\tau * u^k$.

2. Set $u^{k+1} := \begin{cases} f, & \text{if} \quad x \in \Omega \setminus D, \\ 1, & \text{if} \quad x \in D \quad \text{and} \quad \big(G_\tau * u^k\big)(x) > 1/2, \\ 0, & \text{otherwise.} \end{cases}$

$k = k+1$.

Remark 3.1. Note that in the derivation, we first use the fact that $(u(x))^2 = u(x)$ for any $u \in B$ at any x to write the equivalent formulation of the original problem and then relax the problem to the minimization of a concave function in a convex set. This can be interpreted as a concave formulation (or approximation) of the objective functional for the $0-1$ optimization problems. Similar ideas can also be seen in [47].

We now show that the sequence generated from Algorithm 1 can unconditionally decay the objective functional in the following theorem.

Theorem 3.1. *Let u^k be the k-th iteration, we have*

$$\tilde{E}^\tau(u^{k+1}) \leq \tilde{E}^\tau(u^k), \quad \forall \tau > 0.$$

Proof. Write

$$L^\tau(f,u^k,u^k) = E^\tau(u^k) - \mu\sqrt{\frac{\pi}{\tau}}\int_\Omega u^k G_\tau * u^k dx - \int_{\Omega\setminus D} f^2 dx,$$

and

$$L^\tau(f,u^k,u^{k+1}) = E^\tau(u^{k+1}) + \mu\sqrt{\frac{\pi}{\tau}}\int_\Omega u^k G_\tau * (u^{k+1}-2u^k) dx - \int_{\Omega\setminus D} f^2 dx.$$

Since $L^\tau(f,u^k,u^{k+1}) \leq L^\tau(f,u^k,u^k)$, we have

$$E^\tau(u^{k+1}) \leq E^\tau(u^k) - \mu\sqrt{\frac{\pi}{\tau}}\int_\Omega \left[G_{\tau/2} * (u^k - u^{k+1})\right]^2 dx.$$

Therefore, we can conclude that ICTM unconditionally satisfies the energy stability. □

3.1 Another equivalent formulation and derivation

Because of the sharp representation of the interface using indicator functions, one can also consider directly expressing the fidelity term as a constraint and formulating the minimization of (2.1) as the following constrained optimization problem by ignoring the factor $\sqrt{\pi/\tau}$:

$$\begin{aligned} &\min_{u\in B} \int_\Omega u G_\tau * (1-u) dx \\ &\text{s.t.} \quad u = f, \quad \forall x \in \Omega\setminus D. \end{aligned} \tag{3.7}$$

This approximate model (3.7) can be interpreted as the minimization of the length between two binary sub-regions in the damaged region such that the interface is consistent with the binary image outside the damaged region. We then write the problem into

$$\min_{u\in\tilde{B}} E^\tau(u) = \int_\Omega u G_\tau * (1-u) dx, \tag{3.8}$$

where

$$\tilde{B} := \{u \in BV(\Omega,R) \,|\, u(x) \in \{0,1\}, \forall x \in D \text{ and } u(x) = f(x), \forall x \in \Omega\setminus D\}.$$

It is easy to see that $\tilde{B}$ is the boundary of its convex hull $\tilde{K}$, which is defined by

$$\tilde{K} := \{u \in BV(\Omega,R) \,|\, u(x) \in [0,1], \forall x \in D \text{ and } u(x) = f(x), \forall x \in \Omega\setminus D\}.$$

Since the minimizer of a concave functional on a convex set can always be attained at the boundary, one can consider the following equivalent problem to (3.8):

$$\min_{u\in\tilde{K}} E^{\tau}(u). \tag{3.9}$$

To solve (3.9), we use the property of the concavity of $E^{\tau}(u)$ to generate an iterative sequence

$$u^1, u^2, \cdots, u^k, \cdots$$

such that

$$u^{k+1} = \arg\min_{u\in\tilde{K}} L^{\tau}(u, u^k), \tag{3.10}$$

where

$$L^{\tau}(u,u^k) = E^{\tau}(u^k) + \int_{\Omega} (u-u^k) G_{\tau} * (1-2u^k)$$

is the linearization of $E^{\tau}(u)$ at $u=u^k$. It is straightforward to check that the minimization of (3.10) can be done in a pointwise manner as

$$u^{k+1}(x) = \begin{cases} 1, & \text{if} \quad \left(G_{\tau} * (1-2u^k)\right)(x) < 0, \\ 0, & \text{otherwise}, \end{cases} \qquad \forall x \in D, \tag{3.11}$$

implying the update step in Algorithm 1.

Remark 3.2. This derivation and formulation are interpreted as reconstructing the interface between binary domains in the damaged domain based on the pattern outside the domain, especially the conditions on the boundary. It implies that threshold dynamics can handle interface motions with a Dirichlet boundary condition in a fixed domain.

4 Numerical results

In this section, we apply Algorithm 1 for binary, greyscale and color images to show the performance. In the implementation, because λ and μ are the parameters which do not have effect in Algorithm 1, we set λ and μ as 1 for simplicity. Consequently, the recovered images are obtained by only choosing proper τ, leading to a significant reduction in the complexity of parameter tuning.

4.1 Objective functional monotonic decay

In this section, we firstly show the evolution process of the interface between two binary regions in the damaged region together with the curve of the objective functional decay. Considering a damaged triangle image (see Fig. 1) as an example, we plot the decay of the objective functional values during iterations from the initial configuration to the final restored result, as shown in Fig. 2. The snapshots at the iterations 1,2,3,5,7 and 10

Figure 1: Left: Original images. Middle: Damaged images. Right: Initial images. See Section 4.1.

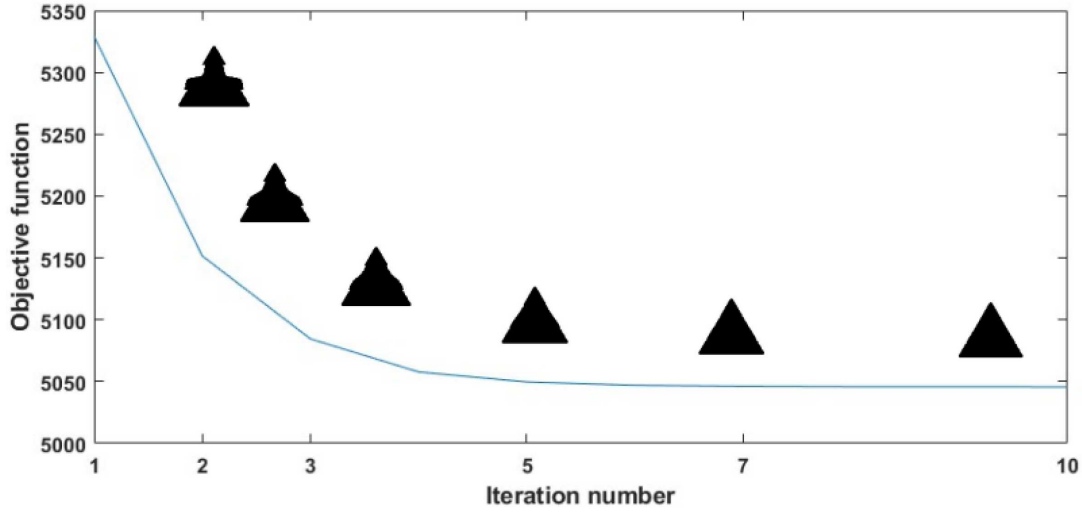

Figure 2: The objective functional value decay curve with snapshots during iterations. See Section 4.1.

are also displayed above the curve of the objective functional. One can observe that the algorithm converges in 10 steps and the objective functional value decays monotonically. This is consistent with Theorem 3.1 and implies the efficiency of the proposed algorithm.

4.2 Comparisons between Algorithm 1 and other algorithms

In this experiment, we mainly use eight damaged images (see Fig. 3) as examples to conduct a comparison between the proposed algorithm and other recent algorithms. To be specific, we compare Algorithm 1 to a convex splitting based method [37], an operator splitting based method [44] and an ALM [43].

We show the results obtained by these four different methods in Figs. 4 and 5, where the four columns are obtained by applying a convex splitting based method, an operator splitting based method, an ALM, and the proposed ICTM, respectively.

From Figs. 4 and 5, one can observe that the proposed ICTM excels from the following several aspects:

1. Boundary preservation: In most restored images, the proposed ICTM and the convex splitting method excel at preserving sharp boundaries in restored images, while

the operator splitting method and the ALM may result in blurred or less defined boundaries in the damaged regions.

2. Blurring reduction: The operator splitting method tends to introduce noticeable blurring in the restored images, and the ALM may show slight blurring in some cases. However, the convex splitting method and the ICTM generally produce sharper images with reduced blurring.

3. Pixel loss and completeness: The convex splitting method and the ALM may lead to the loss of black or white pixels at boundaries, impacting the completeness of restoration. The operator splitting method can sometimes exhibit disconnection or incomplete restoration in damaged areas. The ICTM seems to consistently achieve high-quality restoration, effectively maintaining crucial image information and boundaries, even for the damaged "Circle", where a satisfactory restoration of a curve with constant curvature is obtained.

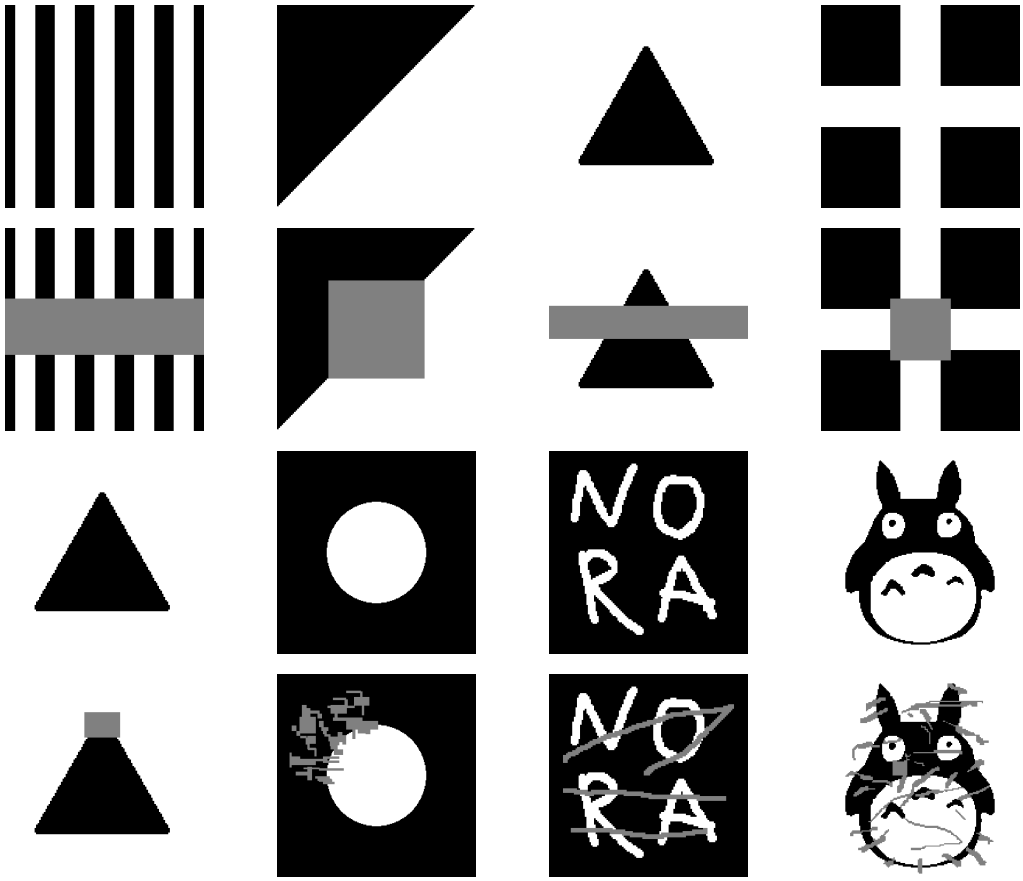

Figure 3: Original images and damaged images. First and third rows: Original images. Second and fourth rows: damaged images. See Section 4.2.

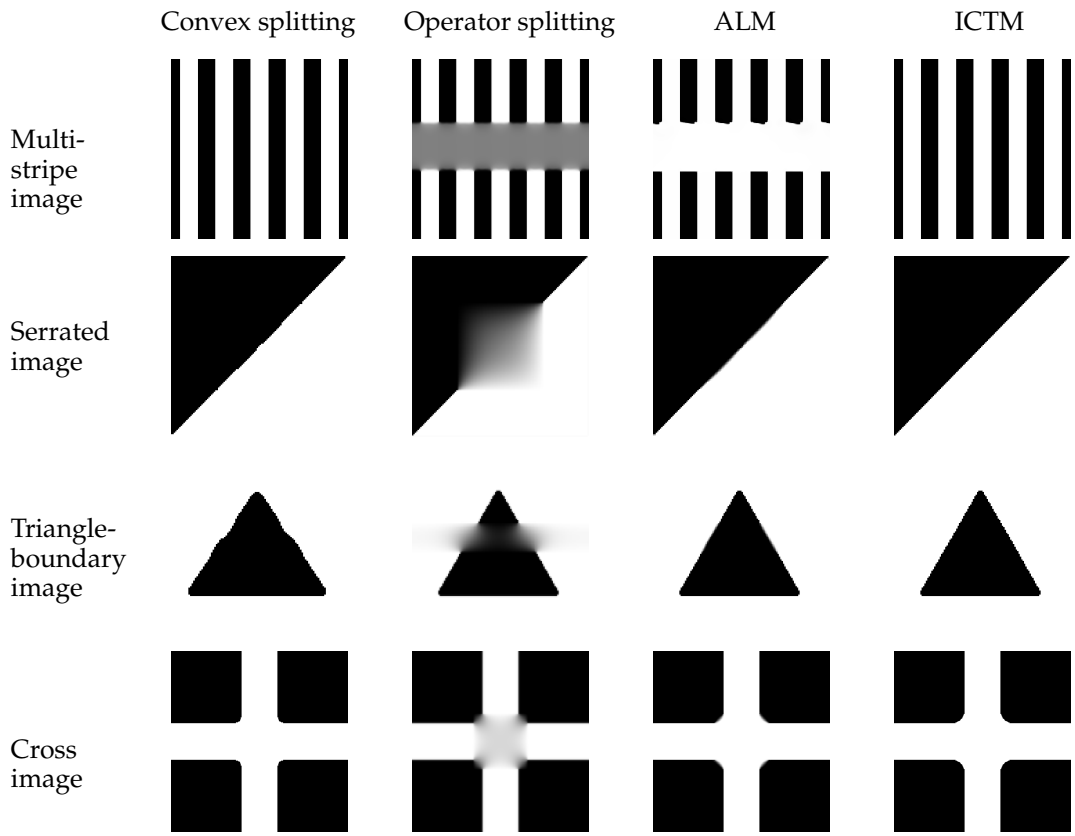

Figure 4: Inpainted images obtained from different methods. First column: Convex splitting method. Second column: Operator splitting method. Third column: ALM. Fourth column: The proposed ICTM. The parameter τ in ICTM is set as 0.03,0.05,0.07 and 0.002 from top to bottom. See Section 4.2.

4.2.1 Some significant indexes

In order to compare the efficiency, we report the CPU time in Table 1 together with the Peak signal-to-noise ratio (PSNR) and relative error in Table 2, where the PSNR is defined as

$$\text{PSNR} = 10 \times \log_{10} \frac{\left(\max(u_{org})\right)^2}{\|u - u_{org}\|^2 / N},$$

and the relative error is defined by

$$\text{Relative error} := \frac{\|u - u_{org}\|}{\|u_{org}\|}$$

with N being the number of pixel of the images, u being the output image and u_{org} being the original clean image. In these tables, bolded font is used to indicate the shortest CPU times, the largest PSNR and the smallest relative error.

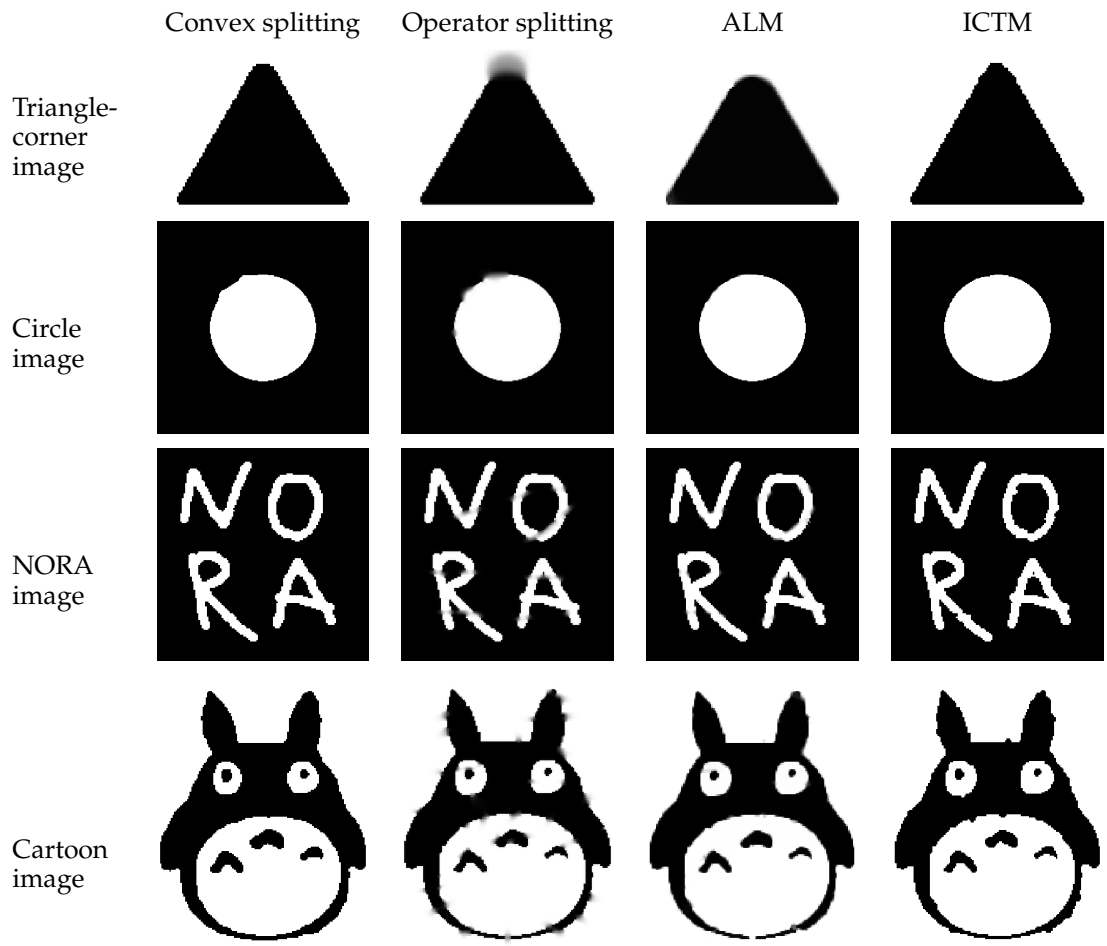

Figure 5: Inpainted images obtained from different methods. First column: Convex splitting method. Second column: Operator splitting method. Third column: ALM. Fourth column: The proposed ICTM. The parameter τ in ICTM is set as 0.004,0.003,0.001 and 0.001 from top to bottom. See Section 4.2.

Table 1: CPU time for the different methods. See Section 4.2.

CPU time	Convex splitting	Operator splitting	ALM	ICTM
Multi-stripe	5.783	73.897	45.334	**0.359**
Serrated	3.318	137.017	18.741	**0.403**
Triangle-boundary	5.468	19.803	5.505	**0.560**
Cross	6.572	19.022	44.156	**1.043**
Triangle-corner	3.199	26.344	18.286	**0.415**
Circle	6.8125	89.300	23.161	**1.218**
NORA	1.831	38.811	9.710	**0.438**
Cartoon	1.517	19.350	13.689	**0.462**

Table 2: PSNR and relative error values for different methods. See Section 4.2.

PSNR (relative error)	Convex splitting	Operator splitting	ALM	ICTM
Multi-stripe	**Inf**(0)	12.948(0.3137)	9.085(0.4893)	**Inf**(**0**)
Serrated	27.373(0.0122)	17.238(0.120)	25.940(0.0246)	**Inf**(**0**)
Triangle-boundary	24.151(0.0229)	22.586(0.0668)	32.633(**0.0093**)	**34.3627**(0.0094)
Cross	**29.357**(**0.0563**)	21.348(0.1167)	23.389(0.1163)	23.883(0.1069)
Triangle-corner	**27.093**(0.0464)	26.467(**0.0420**)	21.344(0.0821)	26.124(0.0466)
Circle	29.134(0.0457)	30.0489(0.0326)	33.9325(0.0225)	**37.0254**(**0.0187**)
NORA	22.799(0.1277)	24.698(0.1114)	**25.213**(**0.0991**)	22.506(0.1240)
Cartoon	14.457(0.0769)	23.111(0.0373)	**23.986**(**0.0272**)	21.386(0.0430)

One can easily see that the ICTM takes the shortest CPU time compared to the other three methods from Table 1. Furthermore, as shown in Table 2, the ICTM produces results that are almost either optimal or second optimal (close to optimal). Inf(0) in Table 2 indicates that the restored image coincides perfectly with the original image, resulting in a PSNR value of infinity and a relative error of zero. These findings highlight the high efficiency of the proposed ICTM.

4.3 Parameter tuning on τ

In this subsection, we delve into the impact of τ on image inpainting. Using "Multi-stripe" image as a case study, we showcase the restored outcomes obtained by employing varying values of τ within the ICTM, as illustrated in Fig. 6. For the damaged "Multi-

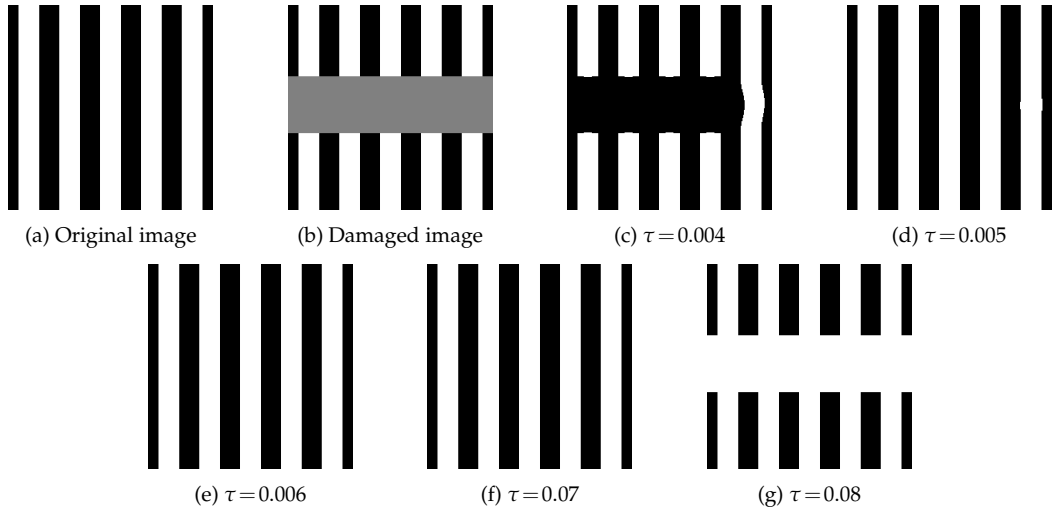

(a) Original image (b) Damaged image (c) $\tau = 0.004$ (d) $\tau = 0.005$

(e) $\tau = 0.006$ (f) $\tau = 0.07$ (g) $\tau = 0.08$

Figure 6: Inpainting the image of "Multi-stripe". (c)-(g) Image inpainting using ICTM with varying τ. See Section 4.3.

stripe" image characterized by sharp boundaries, when τ is small ($\tau=0.004$), the restored image fails to maintain the crisp boundaries, as depicted in Fig. 6(c). Subsequently, as τ increases, the restored images retain their sharp boundaries. However, with a continuous increase in τ, the pixel values within the damaged region converge to one, leading to fragmented boundaries, as shown in Fig. 6(g). Optimal restoration of images can be achieved within a wide range of τ values, typically falling within the range of $[0.006,0.07]$, as demonstrated in Figs. 6(e)-6(f).

In the proposed approximate model, τ measures the accuracy of the approximation. Relatively small values of τ are expected to yield more accurate solutions, while larger values of τ may cause the solution to become more diffused, potentially leading to trivial solutions (e.g. u) being recovered as a constant across the entire damaged region). In the numerical experiment, since the image is defined on fixed pixels, choosing a very small τ may cause the thresholding step in the algorithm to result in no changes, even at a single pixel, during an iteration. As a result, the solution might become "stuck" at a suboptimal state. This is consistent with the observation shown in Fig. 6.

Furthermore, from Figs. 4 and 5 and the percentage of damage as displayed in Table 3, we empirically observe that $\tau \in (0.001,0.004)$ usually gives desired results when damaged percentage falls within $(0,0.1]$ and $\tau \in (0.03,0.07)$ usually gives desired results when damaged percentage falls within $(0.1,0.3)$.

Table 3: Percentage of damage for different damaged images. See Section 4.3.

Image	Multi-stripe	Serrated	Triangle-boundary	Cross
Percentage of damage	0.2734	0.2197	0.1562	0.0905
Image	Triangle-corner	Circle	NORA	Cartoon
Percentage of damage	0.0905	0.0598	0.0766	0.0944

4.4 Integrating the ICTM with other methods

The analysis in Section 4.2 distinctly illustrates the superior efficiency of the proposed ICTM compared to other methods across various images. Nevertheless, when faced with images featuring intricate damage and corner impairments, the ICTM's performance shows a relative weakness. This observation catalyzes the concept of amalgamating ICTM with complementary methodologies to address images with complex damage scenarios and achieve optimal restoration. The proposed strategy entails employing ICTM initially to produce a base restored image efficiently, followed by the application of another technique to refine this output.

Initially, the integration of ALM with ICTM, termed "ICTM-ALM", is employed to restore images like "Cross" and "Triangle-corner". Subsequently, the combination of the operator splitting method with ICTM, known as "ICTM-Operator splitting", is explored for the restoration of "NORA" and "Cartoon" images. The first two rows in Fig. 7 depict

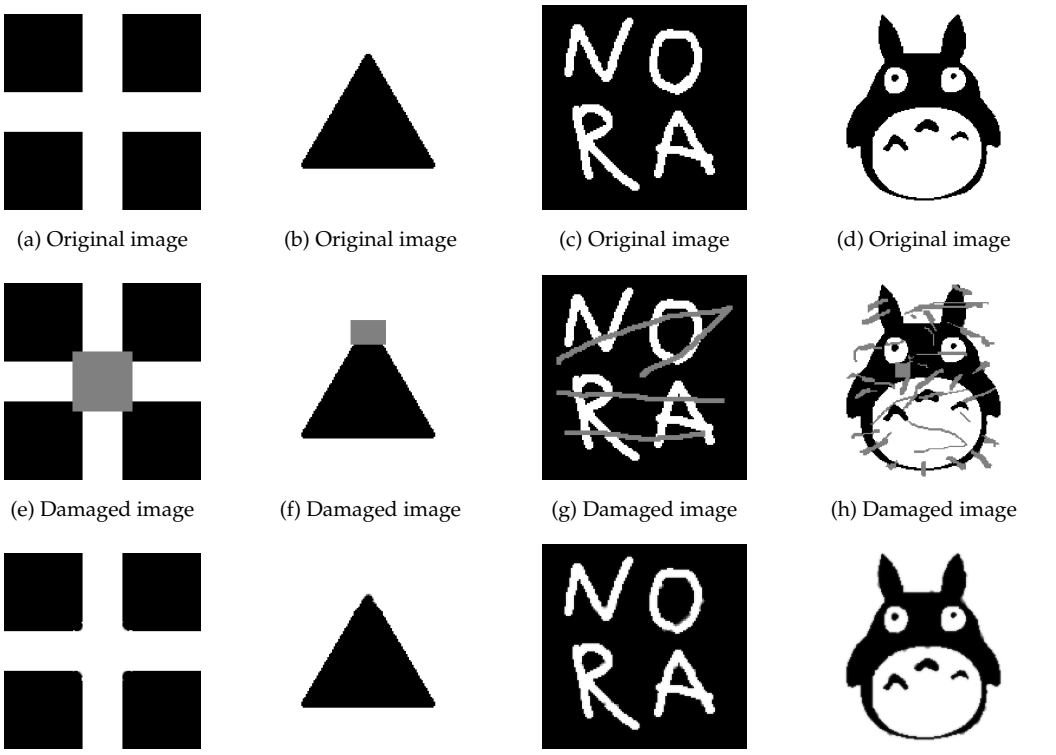

(a) Original image (b) Original image (c) Original image (d) Original image

(e) Damaged image (f) Damaged image (g) Damaged image (h) Damaged image

(i) ICTM-ALM (j) ICTM-ALM (k) ICTM-Operator splitting (l) ICTM-Operator splitting

Figure 7: Using the combined method for image inpainting. See Section 4.4.

the original and damaged images, with the third row showcasing the restored images. The results unequivocally demonstrate the successful preservation of the damaged images' integrity in the restored outputs.

The PSNR and relative error values, alongside the corresponding CPU time costs, are detailed in Tables 4 and 5. Notably, Table 4 highlights that the composite methods (ICTM-ALM and ICTM-Operator splitting) achieve the highest PSNR and lowest relative error values, surpassing the best results outlined in Table 2. In terms of efficiency, the combined

Table 4: PSNR and relative error values for Figs. 7(i)-7(l). See Section 4.4.

PSNR (Relative Error)	Fig. 7(i)	Fig. 7(j)	Fig. 7(k)	Fig. 7(l)
ALM	23.389(0.1163)	21.344(0.0821)	25.213(0.0991)	23.986(0.0272)
Operator splitting	21.348(0.1167)	26.467(0.0420)	24.698(0.1114)	23.111(0.0373)
ICTM	23.883(0.1069)	26.124(0.0466)	22.554(0.1192)	21.386(0.0431)
ICTM-ALM	**30.844**(**0.0464**)	**30.461**(**0.0168**)	–	–
ICTM-Operator splitting	–	–	**25.550**(**0.0854**)	**24.183**(**0.0243**)

Table 5: CPU time for Figs. 7(i)-7(l). See Section 4.4.

CPU	Fig. 7(i)	Fig. 7(j)	Fig. 7(l)	Fig. 7(l)
ALM	44.156	18.286	9.710	13.689
Operator splitting	19.022	26.344	38.811	19.350
ICTM	**1.043**	**0.415**	**0.438**	**0.525**
ICTM-ALM	1.239	0.641	–	–
ICTM-Operator splitting	–	–	0.598	0.653

approaches operate nearly same with the original ICTM concerning CPU time, markedly outperforming both the ALM and operator splitting methods, as demonstrated in Table 5.

4.5 Inpainting of grayscale images

In this subsection, we extend the proposed ICTM to restore greyscale images labeled as "Grey plane", "Grey road" and "Grey people and sea", as depicted in Fig. 8. In the pro-

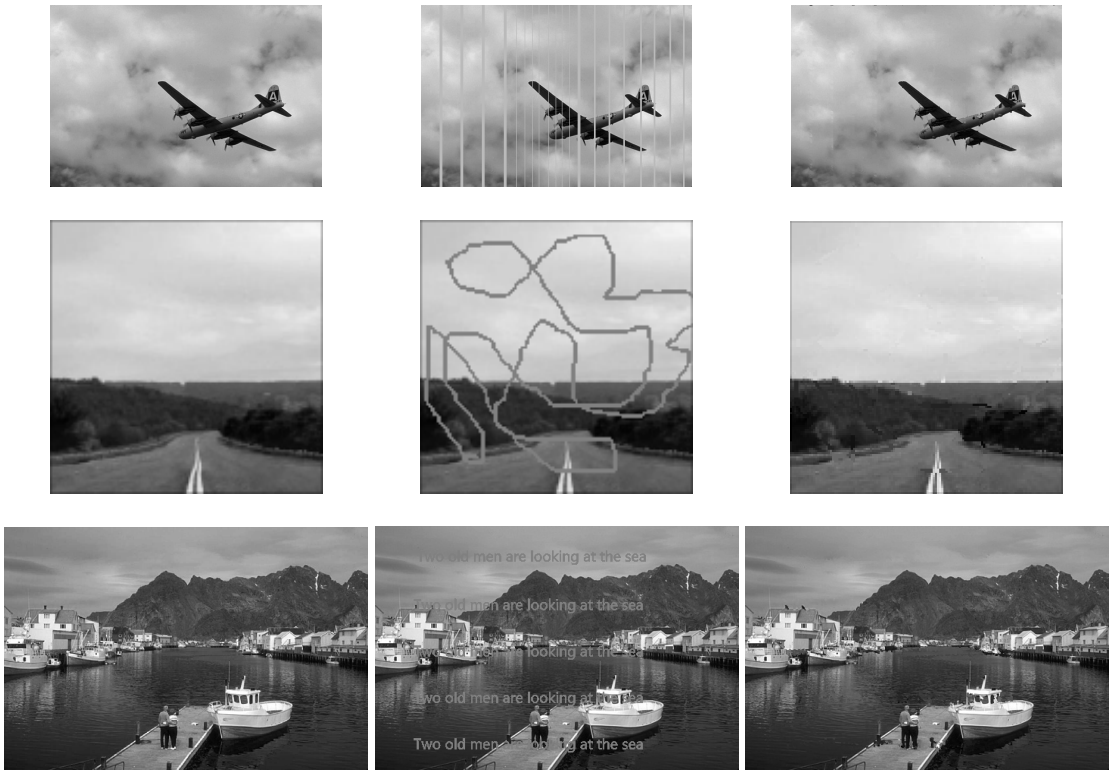

Figure 8: Inpainting the images of "Grey plane", "Grey road" and "Grey people and sea". Inpainting images using ICTM from top to bottom with $\tau = 0.0001, 0.0004, 0.0001$, respectively. See Section 4.5.

cess of recovering the grey images, we adopt the strategy proposed in [40]. The ICTM for grayscale images is to split the image bit-wise into channels using the following approximation:

$$u(x) \approx \sum_{s=1}^{S} u_s(x) 2^{-2(s-1)}, \quad S > 0. \tag{4.1}$$

The ICTM is then applied to each channel, u_s, separately. At the end of the inpainting process, the recovered image is obtained by assembling the inpainting results from all channels. The result is the restored grayvalue image in lower grayvalue resolution. The parameter $S = 8$ is selected based on empirical experience.

The first and second columns in Fig. 8 show the original and damaged images. In the damaged images, the affected areas display vertical lines of varying thickness, curve, and text, respectively. The restored images in the third column of Fig. 8 are obtained by setting the parameter τ to 0.0001,0.0004, and 0.0001, separately. It is clearly demonstrated that the combination of the ICTM method with the employed technique is effective in producing visually satisfactory inpainting results.

4.6 Inpainting the colorful images

In this subsection, we focus on using the ICTM to restore the damaged color images, employing the special strategy (4.1) with $S = 8$.

In Fig. 9, the left column displays the original color images, while the middle column shows the damaged images, with affected areas including hand-draw curves, text, and lines of varying thickness. Setting $\tau = 0.00003, 0.00005, 0.00005$, we get the restored images listed in the right column, demonstrating that the ICTM is capable of producing satisfactory results.

4.7 Image denoising

At the end of this section, we consider to recover the images affected by Gaussian noise. The technique outlined in strategy (4.1) is applied in this example with S set to 8.

In Fig. 10, the left column displays the original images, the middle column presents the images affected by Gaussian noise, and the right column showcases the restored images obtained with τ of 0.0001, 0.00002, and 0.00001. Although the restoration of the penguin's mouth in the middle restored image may not be highly effective, it successfully recovers the overall texture of the scene. The restored images of the peppers in the first image and the sea turtle demonstrate visually satisfactory recovery as well.

5 Conclusion

This paper presents a novel iterative convolution-thresholding method (ICTM) for image inpainting, which produces restored images dependent solely on the parameter τ. We

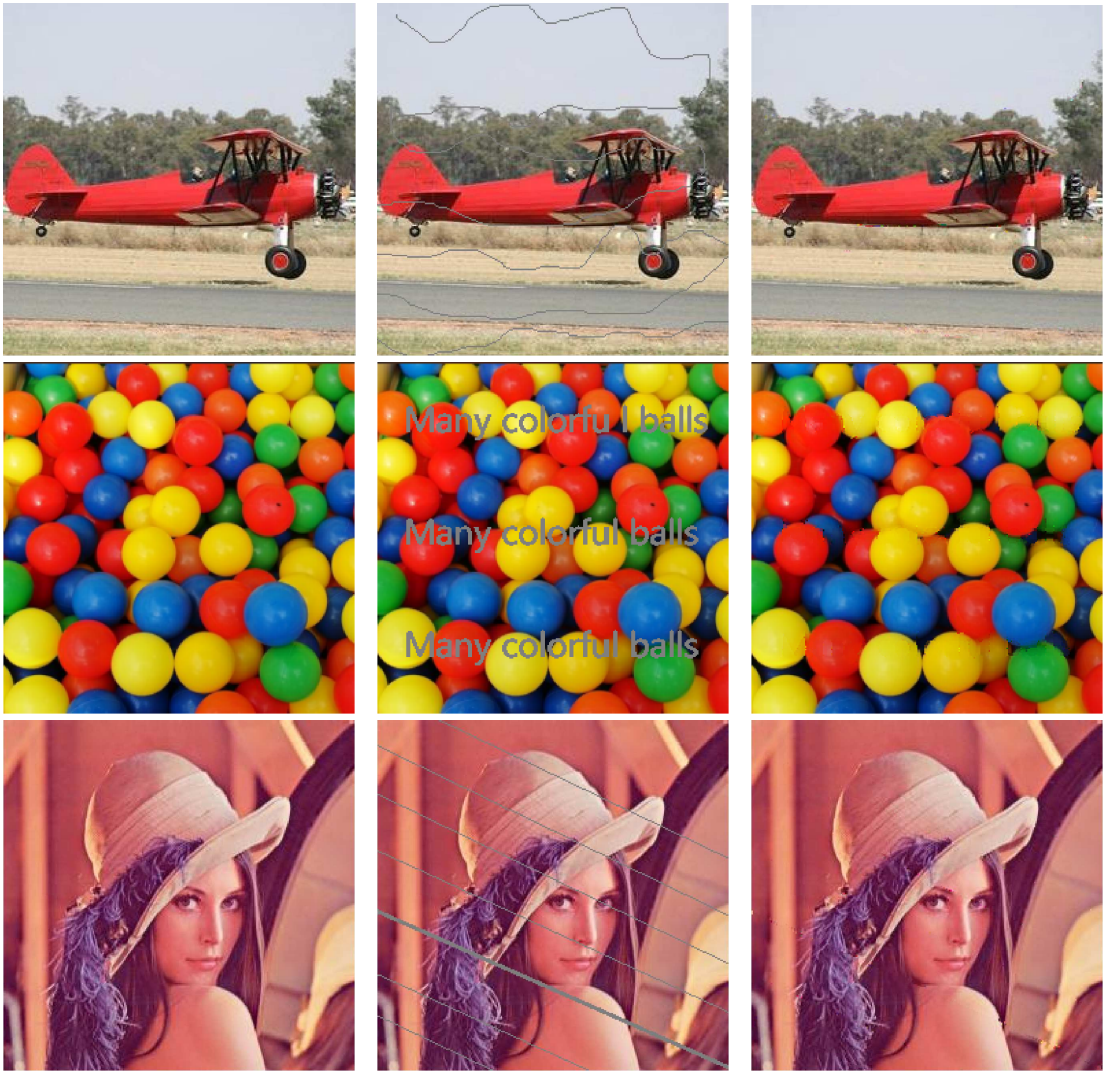

Figure 9: Inpainting the color images of "Airplane", "Ball" and "Lena". Inpainting images using ICTM from top to bottom with $\tau = 0.00003, 0.00005, 0.00005$, respectively. See Section 4.6.

theoretically proved the unconditional monotonically decay of the objective functional, implying the method's stability. Comparative evaluations against traditional methods, such as the convex splitting, augmented Lagrange, and operator splitting-based methods, highlight the ICTM's superior performance, particularly in the efficiency. Analysis of the parameter τ's impact on the recovery process elucidates the method's efficacy. Combining the ICTM with other techniques demonstrates its efficiency and accuracy in addressing complex damage patterns, showcasing the combined approach's potential. We also successfully expanded this method to restore greyscale images, color image, and images corrupted by noise, achieving visually satisfactory results.

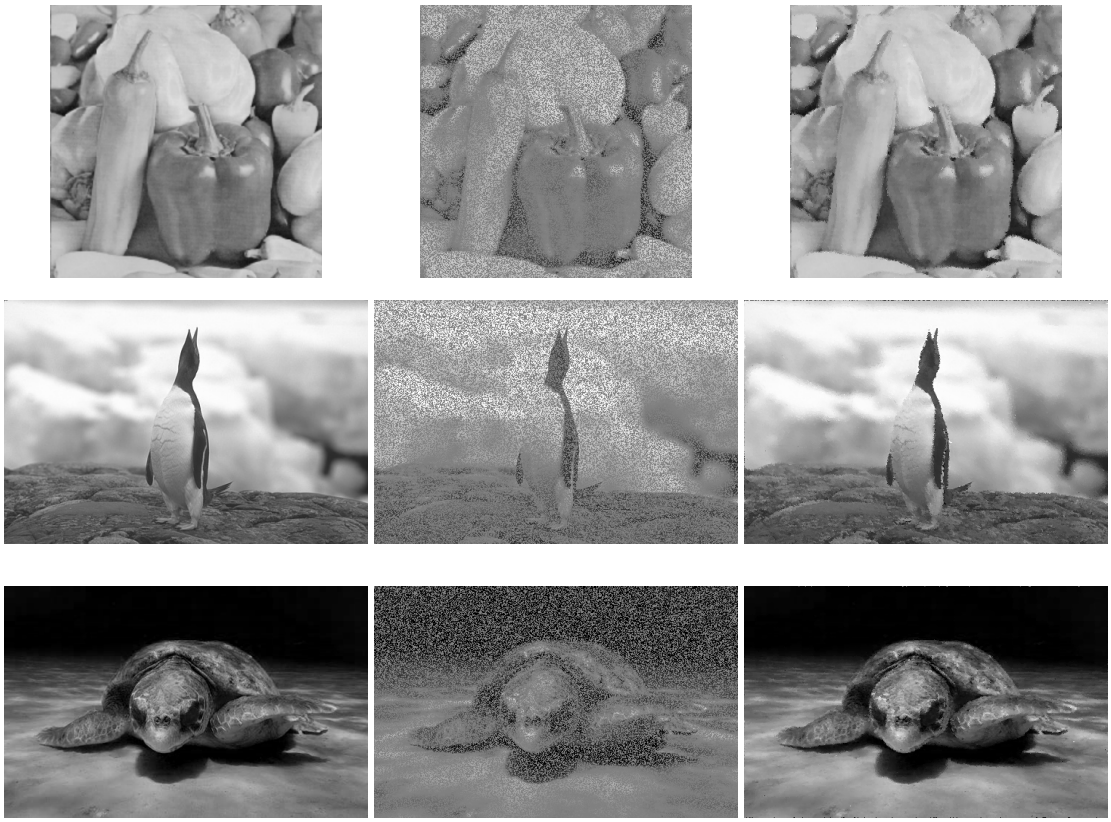

Figure 10: Inpainting the noisy images of "Grey peppers", "Grey penguin" and "Grey sea turtle". Inpainting images using ICTM from top to bottom with $\tau = 0.0001, 0.00002, 0.00001$, respectively. See Section 4.7.

Acknowledgments

We thank Dr. Linlin Tao at Hong Kong Baptist University for providing the MATLAB codes of [44] and Prof. Andrej Novak at University of Zagreb for providing the MATLAB codes of [37].

C. Nan's work is partially supported by the National Science Foundation of China (Grant No. 12501552) and by the Natural Science Foundation of Jiangsu Province (Grant No. BK20250631). D. Wang is partially supported by the National Natural Science Foundation of China (Grant No. 12422116), by the Guangdong Basic and Applied Basic Research Foundation (Grant No. 2023A1515012199), by the Shenzhen Science and Technology Innovation Program (Grant Nos. RCYX20221008092843046, JCYJ20220530143803007), by the Guangdong Provincial Key Laboratory of Mathematical Foundations for Artificial Intelligence (Grant No. 2023B1212010001), and by the Hetao Shenzhen-Hong Kong Science and Technology Innovation Cooperation Zone Project (Grant No. HZQSWS-KCCYB-2024016). Z. Qiao's work is partially supported by the Hong Kong Research

Grants Council (RFS Project No. RFS2021-5S03 and GRF Project No. 15302122) and by the Hong Kong Polytechnic University internal Grant No. 1-9BCT.

References

[1] R. Abergel and L. Moisan, *The Shannon total variation*, J. Math. Imaging Vision, 59:341–370, 2017.
[2] X. Bai, J. Sun, J. Shen, W. Yao, and Z. Guo, *A Ginzburg-Landau-H^{-1} model and its SAV algorithm for image inpainting*, J. Sci. Comput., 96:40, 2023.
[3] M. Bertalmio, A. Bertozzi, and G. Sapiro, *Navier-Stokes, fluid dynamics, and image and video inpainting*, in: Proceedings of the 2001 IEEE Computer Society Conference on Computer Vision and Pattern Recognition, Vol. 1, IEEE, 2001.
[4] M. Bertalmio, G. Sapiro, V. Caselles, and C. Ballester, *Image inpainting*, in: Proceedings of the 27th Annual Conference on Computer Graphics and Interactive Techniques, SIGGRAPH 2000, ACM, 417–424, 2000,
[5] A. Bertozzi, S. Esedöglu, and A. Gillette, *Inpainting of binary images using the Cahn-Hilliard equation*, IEEE Trans. Image Process., 16:285–291, 2007.
[6] C. Braverman, *Photoshop Retouching Handbook*, John Wiley & Sons, 1998.
[7] J.-F. Cai, R. Chan, and Z. Shen, *A framelet-based image inpainting algorithm*, Appl. Comput. Harmon. Anal., 24:131–149, 2008.
[8] F. Cao, Y. Gousseau, S. Masnou, and P. Pérez, *Geometrically guided exemplar-based inpainting*, SIAM J. Imaging Sci., 4:1143–1179, 2011.
[9] L. Cen, W. Hu, D. Wang, and X. Wang, *An iterative thresholding method for the minimum compliance problem*, Commun. Comput. Phys., 33:1189–1216, 2023.
[10] R. Chan, J. Yang, and X. Yuan, *Alternating direction method forimage inpainting in wavelet domains*, SIAM J. Imaging Sci., 4:807–826, 2011.
[11] T. Chan and J. Shen, *Mathematical models of local non-texture inpainting*, SIAM J. Appl. Math., 62:1019–1043, 2002.
[12] H. Chen, P. Dong, D. Wang, and X.-P. Wang, *A prediction-correction based iterative convolution-thresholding method for topology optimization of heat transfer problems*, J. Comput. Phys., 511:113119, 2024.
[13] H. Chen, H. Leng, D. Wang, and X. Wang, *An efficient threshold dynamics method for topology optimization for fluids*, CSIAM Trans. Appl. Math., 3:26–56, 2022.
[14] L. Condat, *Discrete total variation: New definition and minimization*, SIAM J. Imaging Sci., 10:1258–1290, 2017.
[15] L.-J. Deng, R. Glowinski, and X.-C. Tai, *A new operator splitting method for the Euler elastica model for image smoothing*, SIAM J. Imaging Sci., 12:1190–1230, 2019.
[16] L. Dickerman, *Devid King. The commissar vanishes: The falsification of photographs and art in Stalin's Russia*, The Art Bulletin, 80(4):755–757, 1998.
[17] X. Du, D. Cho, and T. Bui, *Image inpainting and segmentation using hierarchical level set method*, in: The 3rd Canadian Conference on Computer and Robot Vision (CRV'06), IEEE, 52–52, 2006.
[18] M. Ebrahimi and E. Lunasin, *The Navier-Stokes-Voight model for image inpainting*, IMA J. Appl. Math., 78:869–894, 2013.
[19] G. Emile-Male, *The Restorer's Handbook of Easel Painting*, Van Nostrand Reinhold, 1976.
[20] S. Esedoğlu and F. Otto, *Threshold dynamics for networks with arbitrary surface tensions*, Commun. Pure Appl. Math., 68:808–864, 2015.

[21] S. Esedoğlu and J. Shen, *Digital inpainting based on the Mumford-Shah-Euler image model*, European J. Appl. Math., 13:353–370, 2002.
[22] Y. Gao and K. Bredies, *Infimal convolution of oscillation total generalized variation for the recovery of images with structured texture*, SIAM J. Imaging Sci., 11:2021–2063, 2018.
[23] J. Haehnle and A. Prohl, *Mumford-Shah-Euler flow with sphere constraint and applications to color image inpainting*, SIAM J. Imaging Sci., 4:1200–1233, 2011.
[24] F. He, X. Wang, and X. Chen, *A penalty relaxation method for image processing using Euler's elastica model*, SIAM J. Imaging Sci., 14:389–417, 2021.
[25] W. Hu, D. Wang, and X.-P. Wang, *An efficient iterative method for the formulation of flow networks*, Commun. Comput. Phys., 31:1317–1340, 2022.
[26] A. C. Kokaram, *Motion Picture Restoration: Digital Algorithms for Artefact Suppression in Degraded Motion Picture Film and Video*, Spring-Verlag, 1998.
[27] C. Li, R. Huang, Z. Ding, J. C. Gatenby, D. N. Metaxas, and J. C. Gore, *A level set method for image segmentation in the presence of intensity inhomogeneities with application to MRI*, IEEE Trans. Image Process., 20:2007–2016, 2011.
[28] J. Li, C. Huang, R. Chan, H. Feng, M. Ng, and T. Zeng, *Spherical image inpainting with frame transformation and data-driven prior deep networks*, SIAM J. Imaging Sci., 16:1177–1194, 2023.
[29] J. Lie, M. Lysaker, and X. Tai, *A variant of the level set method and applications to image segmentation*, Math. Comput., 75:1155–1174, 2006.
[30] C. Liu, Z. Qiao, and Q. Zhang, *Two-phase segmentation for intensity inhomogeneous images by the Allen-Cahn local binary fitting model*, SIAM J. Sci. Comput., 44:B177–B196, 2022.
[31] C. Liu, Z. Qiao, and Q. Zhang, *An active contour model with local variance force term and its efficient minimization solver for multiphase image segmentation*, SIAM J. Imaging Sci., 16:144–168, 2023.
[32] J. Ma, D. Wang, X.-P. Wang, and X. Yang, *A characteristic function-based algorithm for geodesic active contours*, SIAM J. Imaging Sci., 14:1184–1205, 2021.
[33] B. Merriman, J. Bence, and S. Osher, *Diffusion Generated Motion by Mean Curvature*, CAM Report 92-18, University of California, 1992.
[34] M. Miranda, D. Pallara, F. Paronetto, and M. Preunkert, *Short-time heat flow and functions of bounded variation in* $\mathbf{R}^N$, Ann. Fac. Sci. Toulouse Math., 16(1):125–145, 2007.
[35] D. Mumford and J. Shah, *Optimal approximations by piecewise smooth functions and associated variational problems*, Commun. Pure Appl. Math., 42:577–685, 1989.
[36] C. Nan and Q. Zhang, *Elactic bending total variation model for image inpainting with operator splitting method*, Comput. Math. Appl., 176:150–164, 2024.
[37] A. Novak and N. Reinić, *Shock filter as the classifier for image inpainting problem using the Cahn-Hilliard equation*, Comput. Math. Appl., 123:105–114, 2022.
[38] B. Osting and D. Wang, *Diffusion generated methods for denoising target-valued images*, Inverse Probl. Imaging, 14:205–232, 2020.
[39] L. Rudin, S. Osher, and E. Fatemi, *Nonlinear total variation based noise removal algorithms*, Phys. D, 60:259–268, 1992.
[40] C.-B. Schönlieb and A. Bertozzi, *Unconditionally stable schemes for higher order inpainting*, Commun. Math. Sci., 9:413–457, 2011.
[41] J. Shen, J. Xu, and J. Yang, *The scalar auxiliary variable (SAV) approach for gradient flows*, J. Comput. Phys., 353:407–416, 2018.
[42] J. Shen, J. Xu, and J. Yang, *A new class of efficient and robust energy stable schemes for gradient flows*, SIAM Rev., 61:474–506, 2019.
[43] X.-C. Tai, J. Hahn, and G. Chung, *A fast algorithm for Euler's elastica model using augmented*

Lagrangian method, SIAM J. Imaging Sci., 4:313–344, 2011.

[44] L. Tao, *An Operator Splitting Method for Solving Elastica Model*, PhD Thesis, Hong Kong Baptist University, 2022.

[45] S. Wali, H. Zhang, H. Chang, and C. Wu, *A new adaptive boosting total generalized variation (TGV) technique for image denoising and inpainting*, J. Vis. Commun. Image Represent., 59:39–51, 2019.

[46] D. Wang, *An efficient iterative method for reconstructing surface from point clouds*, J. Sci. Comput., 87:38, 2021.

[47] D. Wang, *An efficient unconditionally stable method for Dirichlet partitions in arbitrary domains*, SIAM J. Sci. Comput., 44:A2061–A2088, 2022.

[48] D. Wang, H. Li, X. Wei, and X.-P. Wang, *An efficient iterative thresholding method for image segmentation*, J. Comput. Phys., 350:657–667, 2017.

[49] D. Wang and X.-P. Wang, *The iterative convolution-thresholding method (ICTM) for image segmentation*, Pattern Recognit., 130:108794, 2022.

[50] D. Wang, S. Zeng, and J. Zhang, *A modularized algorithmic framework for interface related optimization problems using characteristic functions*, arXiv:2206.01876, 2022.

[51] J. Wang, Z. Han, and J. Kim, *An efficient and explicit local image inpainting method using the Allen-Cahn equation*, Z. Angew. Math. Phys., 75:44, 2024.

[52] J. Zhang, K. Chen, and B. Yu, *An iterative Lagrange multiplier method for constrained total-variation-based image denoising*, SIAM J. Numer. Anal., 50:983–1003, 2012.